A study of step defects on NiAl(110) using a curved single crystal surface

Piñeiros Bastidas, J.M.; Auras, S.V.; Juurlink, L.B.F.

Surface Science 732 (2023) 122270

Contents lists available at ScienceDirect

Surface Science

journal homepage: www.elsevier.com/locate/susc

A study of step defects on NiAl(110) using a curved single crystal surface

Jessika M. Piñeiros-Bastidas [a], Sabine V. Auras [a,b], Ludo B.F. Juurlink [a,*]

[a] Leiden Institute of Chemistry, Leiden University, PO Box 9502, Leiden, 2300 RA, The Netherlands
[b] Centro de Física de Materiales, Universidad del Pais Vasco, Paseo Manuel de Lardizabal, 5 – E-20018 Donostia, San Sebastian, Spain

ARTICLE INFO

Keywords:
NiAl (110)
Curved single crystal
STM
Image analysis
Terrace width
Kink formation energy

ABSTRACT

In contrast to common flat single crystal surfaces, curved surfaces provide the opportunity to study a large range of vicinals using only one single crystal. Here, we employ a curved NiAl single crystal surface to study step defects on the (110) plane using scanning tunneling microscopy under UHV conditions and at room temperature. The direction of curvature is chosen to align with the alternating Al and Ni atom rows, and we image the surface at various positions along its curvature. With very few exceptions, we find only monoatomic step heights to occur with local step densities consistent with the expected values along the macroscopically curved surface. We use our home-built Python-based analysis script to analyze STM images and obtain statistical information on step and kink distributions, a.o. it allows us to determine the kink formation energy.

1. Introduction

NiAl is a highly-ordered, corrosion-resistant intermetallic compound with a high melting temperature, good thermal conductivity, and low density. Its crystal structure is of the CsCl type. Therefore, the {110} family of crystal planes consists of alternating rows of either Ni atoms or Al atoms oriented along the [001] directions. Fig. 1(a) shows a section consisting of four unit cells of an ideal (110) terrace. At this common (110) surface, the bulk structure relaxes. The Al rows in the surface plane have been found to lie significantly higher than Ni rows [1].

For research purposes, the NiAl(110) crystal plane is highly valuable and often used to create a nearly atomically flat, thin Al_2O_3 overlayer [2]. Onto this oxide overlayer, which does not have the exact structure of the bulk phase [3], metallic particles may be grown. Such systems mimic heterogeneous catalysts with increased resemblance to actual industrial catalysts in comparison to, e.g., the surfaces of metallic single crystals [4]. The thin Al_2O_3 layer has, therefore, been studied in great detail, a.o. by scanning tunneling microscopy (STM) [5,6] and low-energy electron microscopy (LEEM) [7,8].

While large atomically flat planes of Al_2O_3 may be created from the NiAl(110) plane, defects in the thin oxide overlayer occur. A significant fraction of these defects is oriented along the Ni and Al surface rows [9]. Such surface defects in the overlayer are of interest as they are important to the growth and distribution of particles on oxide overlayers. Although intermediate stages of the oxidation of the NiAl(110) plane have been studied [7], the relation between the orientation of these specific defects in the overlayer and the direction of the underlying row-structure can only be speculated upon. They may, for example, originate from monoatomic step heights on the original ultrahigh vacuum (UHV)-cleaned NiAl(110) surface. Supportive to this hypothesis is the finding that, during the initial oxidation of NiAl(110), oxide 'rods' have been found to run along the substrate [001] direction. These oxide rods can elongate from one substrate terrace to the next by gaining or losing atomic layers [7]. Others reported a reorientation of the substrate step edges during oxidation, which accounts for other relative directions of defects in the Al_2O_3 overlayer [9].

Steps on the clean NiAl(110) surface may be expected to run predominantly along the [001] direction. Fig. 1(b) illustrates such steps. Here, two of them separate three (110) oriented NiAl terraces. The black lines trace the steps that also include several kink defects. These steps have not attracted much attention in scientific studies so far even though they seem to be related to the defects in Al_2O_3 overlayers grown from this surface. For example, it is unknown whether the steps consist (predominantly) of Ni or Al and whether steps of doubled height occur beyond single atom high steps.

The smallest kink in an otherwise straight step along the [001] direction unavoidably turns a Ni-terminated terrace into an Al-terminated terrace and vice versa. This is illustrated in Fig. 1(b) by the left step. The blue lines in Fig. 1(a) show the two possible directions of such a kink. Kinks may also span more than a single atom row. Double, triple, or even longer kinks would also run along [111] directions in {110} planes. A double and a triple length kink are illustrated in the right

* Corresponding author.
E-mail addresses: j.m.pineiros.bastidas@lic.leidenuniv.nl (J.M. Piñeiros-Bastidas), l.juurlink@chem.leidenuniv.nl (L.B.F. Juurlink).

https://doi.org/10.1016/j.susc.2023.122270
Received 12 December 2022; Received in revised form 10 February 2023; Accepted 20 February 2023
Available online 27 February 2023

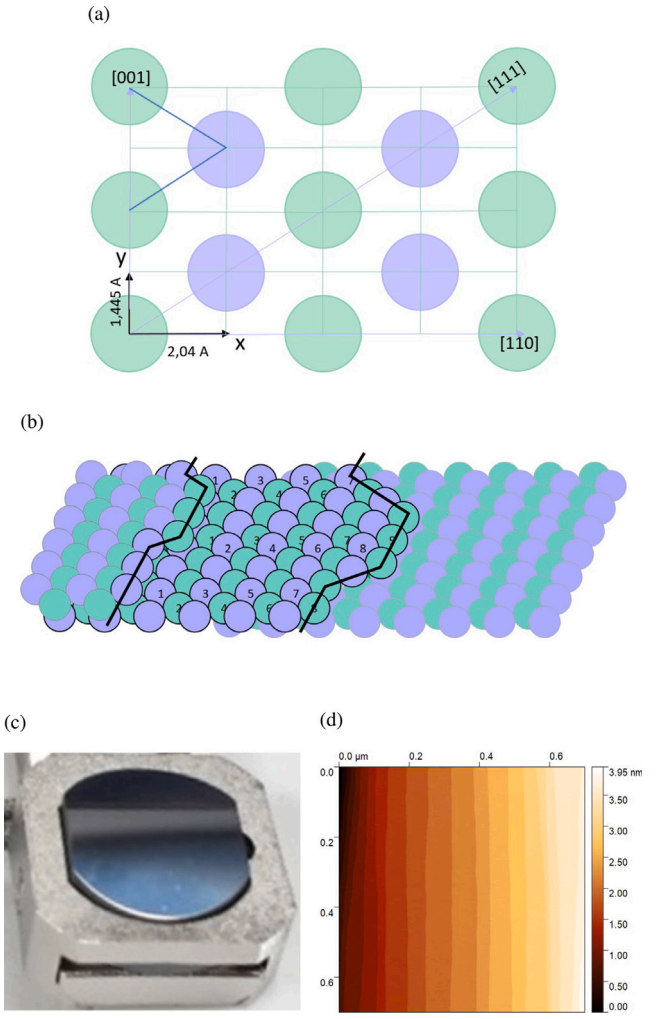

Fig. 1. (a) Schematic representation of the (110) plane on NiAl with the distances between consecutive atoms in x and y directions. The two atom types are depicted using green and purple. Terraces run along the x direction, i.e [110], and steps run along the y direction, i.e., [001]. The blue V-shaped line indicates the two opposing directions of a kink in a step. (b) Schematic representation of a small section of a NiAl(110) surface, including terrace width (a u), two steps and several kink defects. The black lines trace the two kinked step edges . (c) Photograph of the c-NiAl(110)[001] 31° single crystal in a Ni holder. (d) Exemplary STM image taken at room temperature, close to the (110) apex, 700 × 700 nm, feedback 0.2 nA, loop gain 0.53%.

step in Fig. 1(b). Note that kink lengths of even numbers (2, 4, ..) do not result in alteration of the element type that terminates terraces, while odd numbers (1, 3, ..) do. Kinks have also not found significant attention in the literature on NiAl(110) so far. Hence, we do not know whether they are (predominantly) of single atomic length or whether they often occur longer, effectively creating small sections of single atom high steps running along [111]. Such sections may be expected to have considerably higher free energy than edges along [001].

To understand the surface chemical physics of the intermetallic NiAl(110) plane better and its potential relation to defects occurring in an Al_2O_3 overlayer, we study a polished and UHV-cleaned curved surface of a NiAl single crystal. The apex of the curved surface is the (110) plane. The surface may be viewed as a 31° section of a [001] oriented cylinder. The crystal plane is described in the notation suggested by Auras and Juurlink as c-NiAl(111)[001]-31° [10]. The [001] directed macroscopic curvature of the surface is expected to result from monoatomic step heights that occur symmetrically and at increasing frequency when moving away from the (110) apex in either direction. We study NiAl(110) and its continuous range of vicinal surfaces by STM and other surface sensitive techniques.

2. Material and methods

The c-NiAl(110)[001]-31° surface of a NiAl single crystal was created by Surface Preparation Laboratory (Zaandam, the Netherlands). The polished area of the crystal has a radius of curvature of 31°, is 8 mm long, and 7 mm wide. It has a base that reflects the 10 mm diameter NiAl single crystal cylinder from which it was cut by spark erosion. The choice of this size and geometry includes, in principle, all terrace widths ranging from approximately 5 atom row-wide terraces at the edges of the curved surface up to the ideal (110) terrace at the apex. Hence, the distribution of terrace widths smoothly evolves from extremely wide terraces at the apex to very narrow terraces close to the edges of the crystal. The base is used to clamp the crystal to sample holders without inducing significant stress in the surface in various UHV apparatuses. In the photograph presented in Fig. 1(c), we show one of the various types of holders we have developed for such crystals with the macroscopic curvature of the NiAl crystal surface visible. Here, the crystal is accurately held into position onto a Ni base plate by a U-shaped Ni cap. The cap has an opening through which the polished surface protrudes. It also has a small extra opening (appearing on the right side of the polished surface in the photograph) to provide room for a thermocouple, which is laser-welded to the side of the crystal. The cap is held in position by two screws penetrating through the downward legs of the U-shaped cap and into the base plate. To minimize contamination sources, crystal holders are generally constructed from NiAl or Ni. The cleaning procedure of the crystal surface consists of cycles of Ar^+ sputtering (0.7 kV, 2.6 µA, 30 min, under a 45° angle from the apex toward [001]) followed by *in vacuo* annealing (950 K, 5 min).

STM images were taken at room temperature in a UHV VT-STM from Omicron at Centro de Física de Materiales from Universidad del Pais Vasco, a different crystal holder was used there [11]. For analysis purposes, we only use images with 10 to 20 visible terraces. An example is shown in Fig. 1(d). We use Gwyddion [12] for an initial selection of images. These are, subsequently, quantitatively analyzed using a home-built Python script with axes and terrace widths as defined previously [13]. Briefly, the height is defined as the z direction. The y direction runs parallel to the steps, and x runs perpendicular to the steps. The axes are scaled to atomic units (a u) using the distances as illustrated in Fig. 1(a). These are ∼ 2.04 Å along x, i.e., the distance between consecutive atom rows in the (110) plane, and ∼ 1.445 Å along y, i.e., the distance between two consecutive atoms along a step projected onto the [001] axis.

We present results in plots using these atomic units. Counting of terrace widths as rows of atoms is illustrated by the numbers across the middle terrace in Fig. 1(b) at three different locations. Our Python-based script does this for every line of data in the 512 × 512 pixels created for each STM image after determining the exact locations of all downward steps. We include results from sixteen STM images taken at various positions along the curved surface. These sixteen STM images are included in the Supporting Information as Figure S1. It is important to note that our Python script treats each individual terrace in every STM image independently and tracks how its width varies along the y direction per scan line. Statistical analysis is done on collections of such individual terraces. The bin size used to create terrace width histograms is, in principle, the row spacing on the (110) terrace, i.e., ∼ 2.04 Å. The counts are represented at the center of these bins.

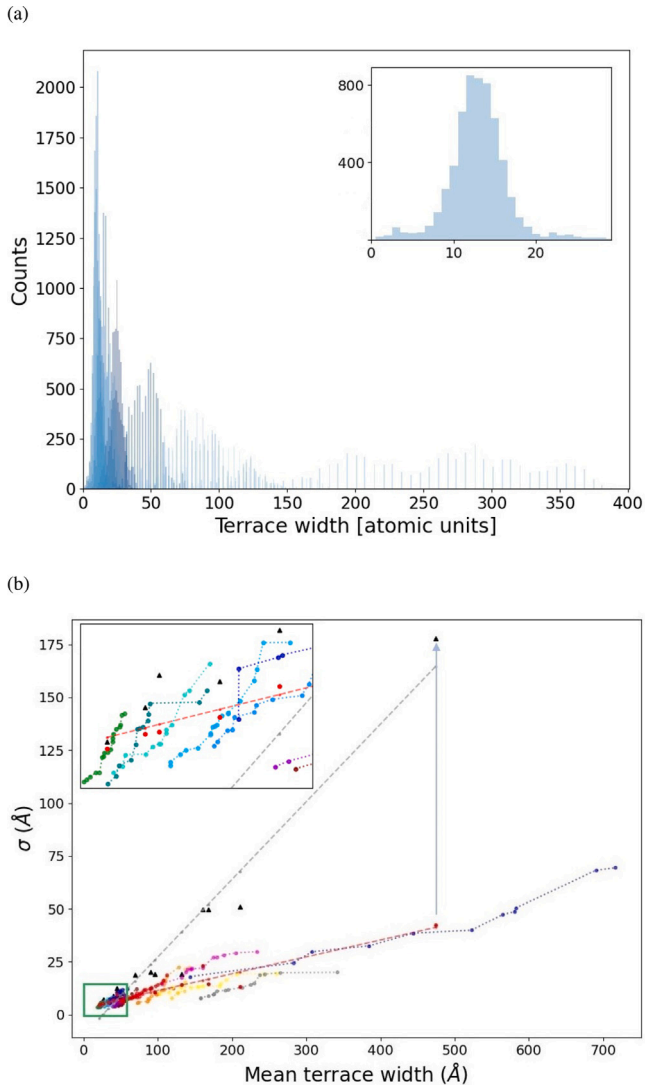

Fig. 2. (a) TWD of sixteen images altogether. The inset shows the TWD for one of the images with the highest resolution. STM image size is 50 nm and it was taken close to one edge of the crystal. (b) Standard deviation vs mean terrace width for all the images analyzed. The inset expands the section shown inside a green rectangle on the bottom left of the plot. Slopes comparison between the image-averaged values (black triangles) and the terrace-averaged values (red circles) are shown with gray and red dashed lines, respectively.

3. Results and discussion

Prior to analyzing the sixteen specific STM images, we have investigated 57 random STM images showing 5 to 30 terraces using line profiles in Gwyddion. As average terrace widths varied in these images, but all include multiple terraces, STM image sizes varied accordingly. In all of these images, we mainly observe monoatomic step heights. Only one STM image taken close to the apex exhibited a double and triple high edge that seems to be the consequence of two nearby contaminants that pin edges locally. They are encircled in the Supporting Information, Figure (S2a). We also observe a few instances of step bunching, grouped curving of steps and other types of defects. Examples are also included in the STM images shown in Figures S3, and S4 in the Supporting Information.

Moving away from the apex, STM images mostly show straight step edges along the y-axis, as illustrated in Fig. 1(d). We visualize the entire analyzed range of data from the sixteen selected images in Fig. 2(a). It plots the terrace width distributions (TWD), i.e., the frequency with which particular terrace widths occur. Clearly, this varies with the distance to the apex. The vertical axis of the plot, labeled as "Counts", represents the number of times we encounter values of terrace widths within the range of bin sizes for each individual image. Mean terrace width values range from 20.75 Å (i.e., 10 a u) to 474.54 Å (232 a u).

There are eight smaller STM images that contribute most of the data ranging up to 40 a u. The STM image size varies between 40 × 40 and 100 × 100 nm^2 for these images. They were taken closer to the edges of the crystal. In the TWDs of these images, we find that both even and odd numbered bins occur. This indicates that terraces must end with rows of both types of elements. If steps would only be formed by one type of element, terraces can only have a width of an odd number of rows. A typical TWD found for one of these eight images is shown in the inset of Fig. 2(a). Neither in this one nor in the others of smaller sized STM images we find a clear systematic variation between even and odd numbered bins. For the image shown in the inset, the ratio of even-to-odd counts is 0.997. Averaged over the 3 images with the highest resolution, it is 0.986.

At the other end of the spectrum, only a single large STM image contributes the data ranging between roughly 175 and 400 a u, but already starting at 27 a u. This image was taken more closely to the (110) apex of the macroscopically curved surface. We excluded some terraces from this latter image because they are incomplete. Such incomplete terraces are visible in Fig. 1(d) at the left and right edges of the image. We analyzed twelve terraces from this large image. The resulting distribution shown in Fig. 2(a) between roughly 175 and 400 a u is certainly not uniform. Meandering of steps in this single image leads to distributions centered at approx 200, 270, and 360 a u. The appearance of separate clusters with narrower distributions is indicative of the stiffness of the step, i.e., steps are much more straight than the complete distribution containing multiple clusters would suggest. The distributions do not merge to the extent that one broad distribution appears.

The data from this image also nicely illustrates the binning of data that occurs for large STM images. The size of this image is 700 nm × 700 nm imaged using 512 × 512 pixels. Scaling this to atomic units gives 6.69 a u per pixel along x (or the inverse 0.15 pixels/a u). Hence, we expect to find counts from this image only every 6.69 a u. That is also what we find in the terrace width histogram of this image. Bins fill in series spaced by 6, 7, and 7 units repetitively. It is rarely altered by spacings of 6, 6, and 7 units. From the spacings in the histogram, we calculate an average of 6.67 bins (a u), which is in near-perfect agreement with the expected scaled value of 6.69 a u based on the image size and number of pixels.

To exemplify how proper treatment of such STM images is essential to extracting useful statistical information, we plot the standard deviation of the terrace width against its mean value for each of the terraces of every image in Fig. 2(b). For comparison to previously published plots of this type, we here use Ångstroms as the x-axis unit. The inset expands the bottom left part of the graph (green rectangle). A single color represents all data of terraces from a single image. Each terrace from a single image is represented by a single small marker. These are connected by a dotted line of the same color, as visible in the inset. We also mark the terrace-averaged values for each image using a red circle. More specifically, it marks the average terrace width and the average standard deviation (σ) for the complete terraces in every image. For comparison, we also show the image-averaged values using black triangles. It marks the values of the average terrace width (i.e., the same as for the red markers) against the standard deviation calculated for the image as a whole. Certainly, this image-averaged σ exceeds the terrace-averaged value. The vertical light blue line illustrates the maximum overestimate for the images that we have analyzed. This factor ranges from 1.05 for the smallest images with narrow terraces to 4.19 for the largest image with the broadest terraces. When we calculate the slope of

the standard deviation vs the mean terrace width for all the images for the image-averaged (gray dashed line) and for the terrace-averaged (red dashed line) data, we obtain values of 0.367 and 0.0799, respectively. The image-averaged slope is 4.6 times larger than the terrace-averaged slope.

Depending on the purpose of research, one or the other value is of interest. When interested in step-step interaction and diffusivity, σ as determined from terrace-averaged values should be used, as σ is directly proportional to the step diffusivity and inversely proportional to steps-repulsive energetic interactions [14,15]. Here, the focus lies on the behavior of individual steps. Using image-averaged values for σ would lead to underestimating the step-step interaction and overestimating the step diffusivity. However, for non-local measurements, e.g., the determination of chemical reactivity of a vicinal surface, one needs to determine the variation in step density (hence terrace widths) and base the analysis on many terraces. Image-averaged values are, in that case, appropriate. It is recommended for those studies to use several STM images to confirm the continuity of the broader distribution.

We find an apparent steeper slope when we analyze the relation between the standard deviation and the average terrace width for single images. This is most clearly visible in the inset of Fig. 2(b). When tracking the data indicated by a single color, hence originating from a single image, the slope appears steeper than the slope resulting from taking all data in the large pane into account. The largest terraces usually meander more than narrow terraces in any single image, resulting in larger standard deviation values. We find this in all analyzed images.

We also analyze step edge meandering at the atomic scale. For this, we generate 'grid-fitted' meandering of step edges by comparing the coordinates of a step with the coordinates of the atomic grid defined for the crystal as previously described in [13]. We initially only include images with the highest resolution, i.e., images with a maximum size of 50 x 50 nm^2. These images have at least two pixels per atomic unit, preventing significant aliasing in the data. From the 'grid-fitted' images, we analyze the kink lengths. Fig. 3(a) presents a histogram obtained for the set of 3 STM images with the highest resolution. The plot shows the relative occurrence of kinks versus their length in atomic units as measured normal to the step direction. For this crystal structure, this kink length corresponds directly to atoms rows. Kinks of mono-atomic length dominate, indicating step edges switching from Ni- terminated to Al-terminated or vice versa. We find no preference for even numbered kink lengths, which would indicate a preference to maintain the same terrace termination.

For the 'grid-fitted' step edges we discard kinks that are not possible on the atomic grid by verifying the angles of the kinks before making the histogram. The inset in Fig. 3(a) illustrates one step edge as a blue line superimposed on the atomic grid. Here we can see straight sections, monoatomic and diatomic kinks. Kinks directions are also illustrated in Fig. 1(a). There, the two blue lines exemplify what would be considered a monoatomic kink in both directions, which alter the terrace termination from a Ni to an Al atom row and vice versa.

For further kinks analysis, we use the approach described by Zandvliet [16] to calculate the mean square length of a kink $\langle k^2 \rangle$, i.e., the mean of the sum of the squared deviations from a perfectly straight edge, as a function of the unit length taken along the step, r. For clarification, r is the distance unit between points along the step direction used to calculate the mean of the sum of the squared deviations $\langle (x_0 - x_r)^2 \rangle$. Values of $\langle k^2 \rangle$ can easily be extracted from the distribution of kinks along steps by our Python script [13].

Results are shown in Fig. 3(b) for a set of 11 STM images on which we can perform the mean squares displacement analysis. We discriminate in the data between 3 images with the highest resolution (darker colored data), i.e., > 2 pixels/a u, and the remaining eight images with resolution varying down to 0.15 pixels/a u (lighter colored data). Error bars have been included to show the broadening of the data

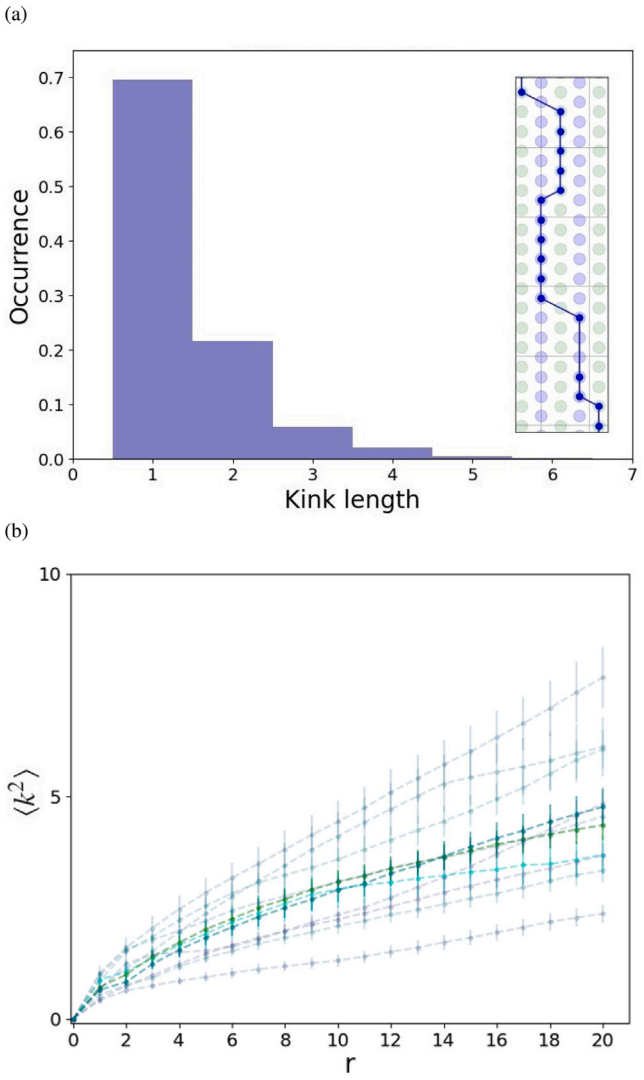

Fig. 3. (a) Kink length distribution histogram as a percentage vs kink length in atomic units. The inset shows a small section of the atomic grid and illustrates 1, and 2 a u length kinks. The green and blue circles represent the two atom types in the NiAl(110) surface. (b) Mean square displacement, $\langle k^2 \rangle$, vs unit length, r, along the step. Darker colored data is taken from high resolution STM images. Lighter colored data has less than atomic resolution. Error bars are included.

dispersion between these two sets of images, darker and lighter colored data.

Fitting the slopes of these lines yields the kink formation energy. We find an average value of 61 ± 3.7 meV for the subset of 3 images with the highest resolution and 60 ± 9.7 meV for the eight images with a resolution up to 0.5 pixels/a u. Undoubtedly, higher resolution images yield a more accurate value with the smallest error. However, the same average is obtainable with a larger margin of error using images with slightly lower resolution.

We are only aware of earlier calculations based on the embedded atom method (EAM) of kink formation energy for a Ni(110) surface. There, 319 meV for the open [110] steps was found and 53 meV for the close-packed [001] steps at 0 K. [17] We are not aware of calculations or measurements on the intermetallic NiAl and we supply the determined value of 61 meV as a benchmark for a future theoretical study. Clearly, it approaches the value predicted for the most comparable, i.e., close-packed step of Ni(110).

4. Conclusion

In this study, we analyzed the curved surface of a NiAl single crystal under UHV conditions by STM. We focused on determining TWDs and analyzing steps and kinks. We found that the surface's macroscopic curvature results only from monoatomic step heights. These predominantly meander along the intended direction of the alternating rows of Ni or Al atoms in the (110) plane.

From the analysis of kinks, we find a preference for monoatomic kinks. We extracted the kink formation energy from the highest resolution images and showed that much larger STM images with an intrinsically low spatial resolution still allow extracting the correct kink formation energy, albeit with a larger margin of error. The kink formation energy along the rows of the NiAl(110) surface resembles that of a pure Ni(110) plane, but this may be fortuitous. Note that our analysis of kinks on the NiAl(110) surface yields an average kink formation energy for both types of kinks, i.e., Ni steps ending and going terrace inward or outward to an Al row. These are obviously the same as Al rows ending and stepping either terrace outward or inward to a Ni row. Hence, the kink formation energy does not inform us of the identity of the elements forming steps.

From the terrace width analysis, there are two remarks depending on the research purpose. If the focus lies on step diffusivity and step-step interactions, σ as determined from terrace-averaged values should be used. If, instead, the focus lies on the surface chemistry, the variation in step density is more relevant and image-averaged values of σ yield the appropriate information. The lack of a strong preference for either even or odd terrace lengths in the TWDs may easily be mistaken to suggest that both elements occur in equal ratios in the step edges. This conclusion is incorrect. Only for terraces with even numbers of rows, we are sure that the terrace terminating elements are equally distributed. For a terrace with an odd number of rows at the scan line, a single element occurs on consecutive steps, but we do not know whether it is (predominantly nor exclusively) Ni of Al. Hence, the total occurrence of one element to the other in step edges cannot be determined from this analysis. However, the fact that TWDs contain both odd and even numbers indicates that both elements must be terminating terraces. The predominant occurrence of single atom length kinks confirms this point. Atomically resolved STM images or a step-specific elemental analysis may provide more detail.

CRediT authorship contribution statement

Jessika M. Piñeiros-Bastidas: Conceptualization, Validation, Formal analysis, Investigation, Writing – original draft, Visualization. **Sabine V. Auras:** Investigation, Writing – review & editing. **Ludo B.F. Juurlink:** Conceptualization, Validation, Writing – review & editing, Supervision.

Declaration of competing interest

The authors declare that they have no known competing financial interests or personal relationships that could have appeared to influence the work reported in this paper.

Data availability

Data will be made available on request.

Acknowledgments

We are greatly indebted to Prof. Dr. Enrique Ortega for allowing S.A. to collect the used STM images in his laboratory and Max Ilyn for experimental guidance. We also kindly thank Prof. Dr. H. J. W. Zandvliet for useful discussions. The research is funded by STW (now TTW) project #15281 of the Dutch Research Council (NWO).

Appendix A. Supplementary data

Supplementary material related to this article can be found online at https://doi.org/10.1016/j.susc.2023.122270.

References

[1] H.L. Davis, J.R. Noonan, Rippled relaxation in the (110) surface of the ordered metallic alloy NiAl, Phys. Rev. Lett. 54 (1985) 566–569, http://dx.doi.org/10.1103/PhysRevLett.54.566, URL https://link.aps.org/doi/10.1103/PhysRevLett.54.566.

[2] R. Jaeger, H. Kuhlenbeck, H.-J. Freund, M. Wuttig, W. Hoffmann, R. Franchy, H. Ibach, Formation of a well-ordered aluminium oxide overlayer by oxidation of NiAl(110), Surf. Sci. (ISSN: 0039-6028) 259 (3) (1991) 235–252, http://dx.doi.org/10.1016/0039-6028(91)90555-7, URL http://www.sciencedirect.com/science/article/pii/0039602891905557.

[3] G. Kresse, M. Schmid, E. Napetschnig, M. Shishkin, L. Köhler, P. Varga, Structure of the ultrathin aluminum oxide film on NiAl(110), Science 308 (5727) (2005) 1440–1442, http://dx.doi.org/10.1126/science.1107783, URL https://www.science.org/doi/abs/10.1126/science.1107783.

[4] H.-J. Freund, G. Pacchioni, Oxide ultra-thin films on metals: new materials for the design of supported metal catalysts, Chem. Soc. Rev. 37 (10) (2008) 2224–2242.

[5] R.-P. Blum, D. Ahlbehrendt, H. Niehus, Growth of Al_2O_3 stripes in $NiAl(001)$, Surf. Sci. (ISSN: 0039-6028) 396 (1) (1998) 176–188, http://dx.doi.org/10.1016/S0039-6028(97)00667-5, URL http://www.sciencedirect.com/science/article/pii/S0039602897006675.

[6] K. Højrup Hansen, T. Worren, E. Lægsgaard, F. Besenbacher, I. Stensgaard, Bias dependent apparent height of an Al_2O_3 thin film on NiAl (110), and of supported Pd clusters, Surf. Sci. (ISSN: 0039-6028) 475 (1) (2001) 96–102, http://dx.doi.org/10.1016/S0039-6028(00)01077-3, URL https://www.sciencedirect.com/science/article/pii/S0039602800010773.

[7] J.P. Pierce, K.F. McCarty, Self-assembly and dynamics of oxide nanorods on NiAl(110), Phys. Rev. B 71 (2005) 125428, http://dx.doi.org/10.1103/PhysRevB.71.125428, URL https://link.aps.org/doi/10.1103/PhysRevB.71.125428.

[8] H. Qin, X. Chen, L. Li, P.W. Sutter, G. Zhou, Oxidation-driven surface dynamics on NiAl(100), Proc. Natl. Acad. Sci. USA 112 (2) (2015) E103–E109, http://dx.doi.org/10.1073/pnas.1420690112.

[9] L. Heinke, L. Lichtenstein, G.H. Simon, T. König, M. Heyde, H.-J. Freund, Structure and electronic properties of step edges in the aluminum oxide film on NiAl(110), Phys. Rev. B 82 (2010) 075430, http://dx.doi.org/10.1103/PhysRevB.82.075430, URL https://link.aps.org/doi/10.1103/PhysRevB.82.075430.

[10] S.V. Auras, L.B. Juurlink, Recent advances in the use of curved single crystal surfaces, Progr. Surf. Sci. (ISSN: 0079-6816) 96 (2) (2021) 100627, http://dx.doi.org/10.1016/j.progsurf.2021.100627, URL https://www.sciencedirect.com/science/article/pii/S0079681621000150.

[11] Nanophysics Lab, Chemical Physics of Complex Materials, Materials Physics Center, 2012, https://cfm.ehu.es/.

[12] D. Nečas, P. Klapetek, Gwyddion: an open-source software for SPM data analysis, Central Eur. J. Phys. (ISSN: 1895-1082) 10 (2012) 181–188, http://dx.doi.org/10.2478/s11534-011-0096-2.

[13] J.M. Piñeiros-Bastidas, S.V. Auras, L.B. Juurlink, A Python script to automate STM image analysis for stepped surfaces, Appl. Surf. Sci. (ISSN: 0169-4332) 567 (2021) 150821, http://dx.doi.org/10.1016/j.apsusc.2021.150821, URL https://www.sciencedirect.com/science/article/pii/S0169433221018845.

[14] E.D. Williams, Surface steps and surface morphology: understanding macroscopic phenomena from atomic observations, Surf. Sci. (ISSN: 0039-6028) 299–300 (1994) 502–524, http://dx.doi.org/10.1016/0039-6028(94)90678-5, URL http://www.sciencedirect.com/science/article/pii/0039602894906785.

[15] H.-C. Jeong, E.D. Williams, Steps on surfaces: experiment and theory, Surf. Sci. Rep. (ISSN: 0167-5729) 34 (6) (1999) 171–294, http://dx.doi.org/10.1016/S0167-5729(98)00010-7, URL https://www.sciencedirect.com/science/article/pii/S0167572998000107.

[16] H.J. Zandvliet, Energetics of Si(001), Rev. Modern Phys. (ISSN: 0034-6861) 72 (2) (2000) 593–602, http://dx.doi.org/10.1103/RevModPhys.72.593, URL https://journals.aps.org/rmp/abstract/10.1103/RevModPhys.72.5930.

[17] C.-L. Liu, J.B. Adams, Step and kink formation energies on fcc metal surfaces, Surf. Sci. (ISSN: 0039-6028) 294 (3) (1993) 211–218, http://dx.doi.org/10.1016/0039-6028(93)90109-W, URL http://www.sciencedirect.com/science/article/pii/003960289390109W.